High-Performance Atomistic Modeling of Evaporation of Thin Films Under Intense Laser Irradiation

Fedor Grigoriev(✉), Vladimir Sulimov, and Alexander Tikhonravov

Research Computing Center, M.V. Lomonosov Moscow State University, Leninskie Gory, Moscow 119234, Russia
vs@dimonta.com, tikh@srcc.msu.ru

Abstract. This paper presents the results of high-performance atomistic modeling of heating and the initial stage of evaporation of thin silicon dioxide films under the action of high-power laser radiation. Both dense isotropic films obtained by normal deposition and highly porous anisotropic silicon dioxide films obtained by deposition at a large angle to the substrate are investigated. The dependence of the initial stage of film evaporation on its structural properties is analyzed.

Keyword: Atomistic modeling · Silicon dioxide films · High-performance simulations · Laser irradiation

1 Introduction

Thin film optical coatings are important elements of high intensity laser installations, among which the most impressive examples are petawatt laser systems used in nuclear fusion plants [1–3]. The main limiting factor preventing a further increase in lasers power is the laser induced damage in thin films of optical coatings [4–6]. The issue of increasing the laser radiation resistance of optical thin films has been on the agenda for more than three decades. To date, experimental methods for studying the laser induced damage in thin films are well developed and described by international standards [7]. At the same time, the general theoretical understanding of the physical mechanism of laser induced damage is still very far from what is desired. But such an understanding is vital for further progress in many critical areas requiring the use of powerful lasers.

Recently, molecular dynamics methods have been actively used to study the interaction of laser irradiation with various materials [8–11], including their heating and subsequent evaporation. These processes play an important role in laser damage [12]. For optical coatings, one of the most important thin film materials is silicon dioxide. The study of heating SiO_2 films under intense laser irradiation was begun in Ref. [13]. This article presents the latest results in this direction.

V. Voevodin and S. Sobolev (Eds.): RuSCDays 2021, CCIS 1510, pp. 114–124, 2021.
https://doi.org/10.1007/978-3-030-92864-3_9

2 Method

Following [14–16] we assume that the absorption of the high-energy laser irradiation occurs due to nonlinear processes such as multiphoton absorption. The process of the interaction of electron subsystem with laser irradiation is not considered explicitly within the framework of this paper, but is taken into account trough the simulation parameters. The transfer of energy from the electronic sub-system of to the nuclei is a short-time process. In our simulations, this transfer is considered as a rapid, almost instantaneous increase in the nuclei kinetic energy. After this moment, the further nuclei moving are considered using the classical molecular dynamics (MD). The energy of interatomic interactions is calculated in the frame of the DESIL force field [17]:

$$U = q_i q_j / r_{ij} + A_{ij} / r_{ij}^{12} - B_{ij} / r_{ij}^{6} \tag{1}$$

where $q_{i(j)}$ is the charge of the $i(j)$-th atom, $q_O = -0.5 q_{Si} = -0.65$e, A_{ij} and B_{ij}, are parameters of the Lennard-Jones potential for the van der Waals interaction, r_{ij} is the interatomic distance, $A_{SiO} = 4.6 \cdot 10^{-8}$ kJ·(nm)^{12}/mol, $A_{SiSi} = A_{OO} = 1.5 \cdot 10^{-6}$ kJ·(nm)^{12}/mol, $B_{SiO} = 4.2 \cdot 10^{-3}$ kJ·(nm)^{6}/mol, $B_{SiSi} = B_{OO} = 5 \cdot 10^{-5}$ kJ·(nm)^{6}/mol.

The atomistic clusters, representing the thin film, were obtained in our previous works [18, 19] using the step-by-step procedure. At each step, silicon and oxygen atoms with stoichiometric proportion of 1:2 are inserted randomly at the top of the simulation box. The initial values of the silicon and oxygen atoms kinetic energies are $E(\mathrm{Si}) = 10$ eV and $E(\mathrm{O}) = 0{,}1$ eV, which corresponds to the high-energy deposition processes. The initial velocities of the oxygen and silicon atoms are directed to the substrate at the deposition angle α (Fig. 1) The *NVT* (constant number of particles, volume and temperature) ensemble is used at every injection step. The vertical dimension of the simulation box is increased by 0.01 nm after each injection step in order to compensate for the growth of film thickness. The duration of one injection step is 10 ps and the time step of MD modeling is 0.5 fs.

The atomistic clusters were deposited at two different deposition angles $\alpha = 0$ and 70°. Deposition at $\alpha = 0$ leads to the formation of dense and homogeneous films, while deposition at large values of α leads to the formation of porous and anisotropic structures (Fig. 1). In this work, we investigate the differences in the heating and evaporation processes for these cases.

The MD simulation of the film heating is organized as described in [13]. At the initial moment, the atoms of the films acquire additional kinetic energy, which corresponds to the following exponentially decreasing temperature distribution over the cluster thickness:

$$\begin{aligned} T(x) = \frac{T_m}{e-1}\left(e^{\left(\frac{2x}{L}-1\right)} - 1\right) + T_0 \text{ if } L/2 < x \le L \\ T(x) = T_0, \text{ if } 0 \le x \le L/2. \end{aligned} \tag{2}$$

Here $T_0 = 300$ K is the film and substrate temperature before the laser radiation absorption, L is the film thickness, T_m is the maximum temperature at the upper edge of

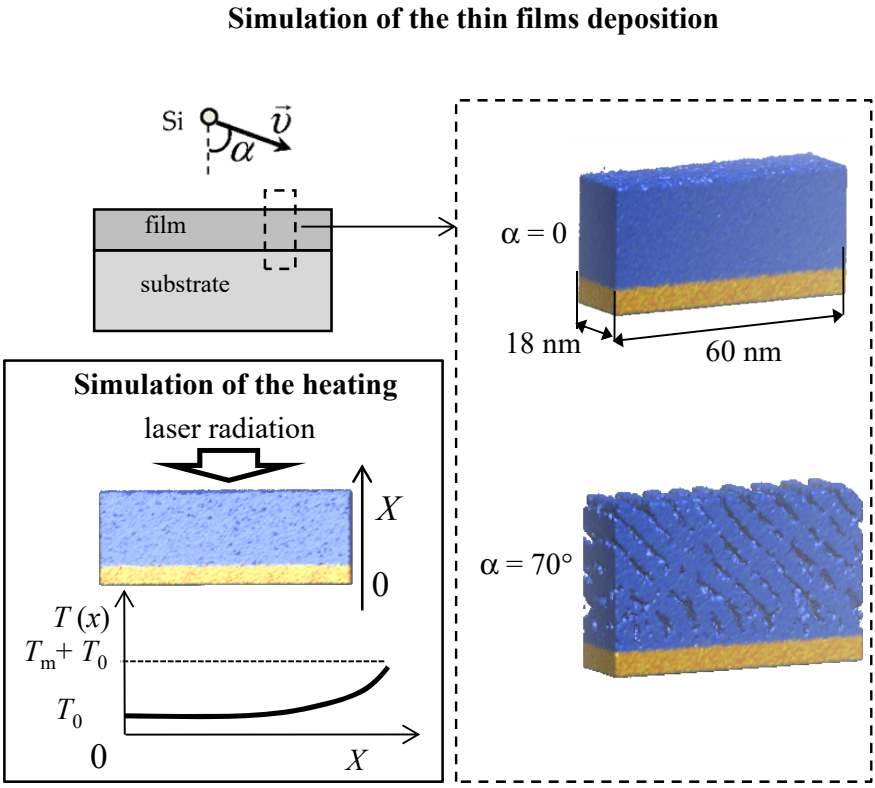

Fig. 1. Scheme of the molecular dynamic simulation of the thin film deposition and heating of the film.

the film. This temperature distribution is schematically shown in Fig. 1. In the present work the T_m value varies from $3 \cdot 10^3$ K to $1.2 \cdot 10^4$ K. At such temperatures, activation of the evaporation process can be expected, since the boiling point for quartz is about of $3 \cdot 10^3$ K [20]. The T_0 value is equal to room temperature, 300 K. The substrate temperature is maintained at T_0 during heating and evaporation using the Berendsen thermostat [21]. The simulations are carried out in the *NVT* ensemble, periodic boundary conditions are applied in all directions. The evaporated atoms can move in the empty volume above the cluster surface.

The duration of the simulation trajectories is about of several tens of picoseconds. This duration is enough to describe the initial stage of the evaporation process.

MD simulations are performed using the GROMACS program [22].

3 Results and Discussion

Films deposited at large angles of incidence α are characterized by the formation of specific structures like slanted columns [23, 24]. These columns are shown in Fig. 1. Since the horizontal dimension of columns exceeds several nanometers, the clusters having at least one dimension equal to several tens of nanometers are needed for the simulation. Therefore, in this work the horizontal dimensions of the substrate are 18 nm and 60 nm (see Fig. 1).

At the end of the simulation of the deposition process, the total number of atoms in the clusters is about of $2.5 \cdot 10^6$. The effective simulation with such number of atoms can be carried out only using parallel calculations. In this work, all simulations are carried out on the supercomputer "Lomonosov-2" of HPC computing resources at Lomonosov Moscow State University [25]. The calculations efficiency is investigated for two main queues available for users: «compute» and «pascal». The processors with following characteristics are used: Intel Haswell-EP E5-2697v3, 2.6 GHz, 14 cores with graphics accelerator NVidia Tesla K40M («compute») and Intel Xeon Gold 6126, 2.6 GHz, 12 cores with graphics accelerator 2 x Nvidia P100, 3584 cuda cores, 16 GB («pascal»), for the further details see [26]. The effectiveness is investigated for the MD trajectory with duration 10 ps, number of atom is about of $2.5 \cdot 10^6$.

The results of the simulation are presented in Fig. 2a,b. As can be seen from Fig. 2a, the simulation time at $N = 64$ is about ten minutes, which makes it possible to systematically investigate the evaporation process. The calculations are performed faster using the «pascal» queue.

The effectiveness of parallel calculation is calculated as follows:

$$a(N) = Nt_8/(8t_N) \tag{3}$$

where N is the number of cores, t_8 and t_N are the simulation time using 8 and N cores, respectively. As can be seen from Fig. 2b, the values of the effectiveness for both queues are almost identical. The decrease in efficiency with an increase in the number of cores can be caused by an increase in the relative computational cost of non-paralleled processes, such as reading of initial geometry, etc.

The simulation results for heating and evaporation are shown in Figs. 3, 4 and Tables 1, 2 and 3.

The time evolution of the temperature distribution over the film volume after absorption of laser radiation is shown in Fig. 3a,b. The cluster is deposited at an angle $\alpha = 70°$. The value of the maximum temperature T_m at the moment $t = 0$ is 4200 K for the plots in Fig. 3a. At this temperature, the evaporation process has not yet been observed. As can be seen from plots in Fig. 3a, the temperature of the upper edge of the films rapidly decreases from T_m value to approximately 1500 K. This effect is associated with the transfer of a part of the additional kinetic energy to the potential energy [13]. This leads to cooling of the film. After that, the temperature distribution changes insignificantly for several tens of picoseconds. This is due to the fact that the characteristic time τ of thermal energy transfer from hot to cold layers of the cluster is much longer than a picosecond. Indeed, the value of τ can be estimated from the heat

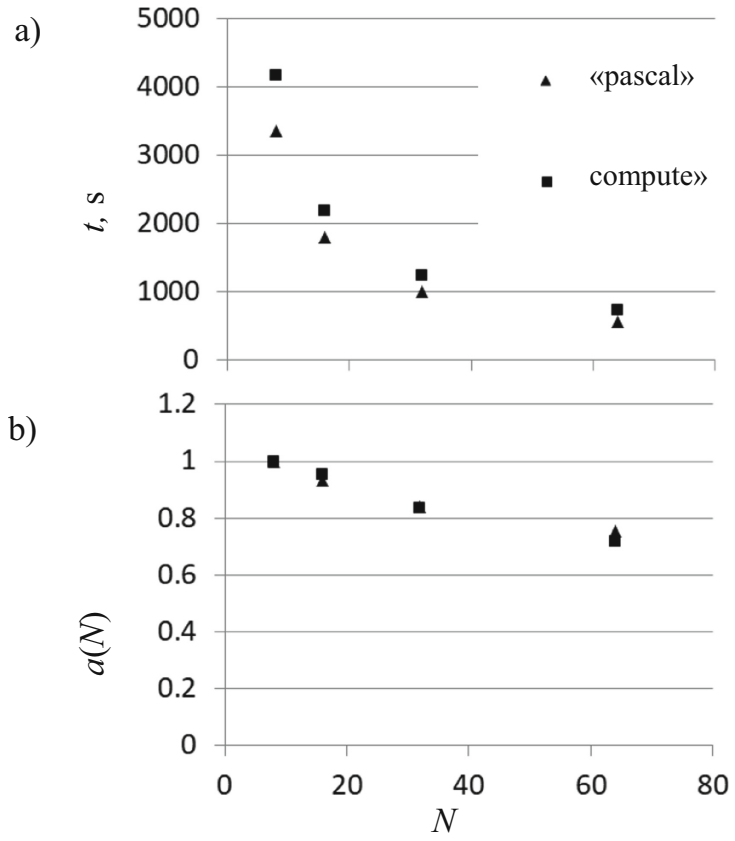

Fig. 2. Dependence of the simulation time t on the number of cores N for queues «compute» and «pascal».

equation as $\tau \sim c\rho L^2/\chi$, where the values of the specific heat capacity, mass density, and heat conductivity are equal to $c = 10^3$ J/(kg·K), $\rho = 2.2 \cdot 10^3$ kg/m^3, and $\chi = 2.0$ W/(m·K) [27]. Since the characteristic cluster thickness L is about 40 nm, we obtain $\tau \sim 1$ ns. In this work, we focused on the investigation of the evaporation process, that occurs in the first few tens of picoseconds (see below). Therefore, we did not study the nanoseconds evolution of temperature profiles.

Temperature distributions at $T_m = 8400$ K are shown in Fig. 3b. As in the case of $T_m = 4200$ K, the temperature rapidly decreases during the firsts picoseconds after the absorption of laser energy. But in this case this decrease is more significant. In addition, a fluctuation of the temperature distribution is observed near the upper edge of the film cluster. These differences are associated with the beginning of the evaporation process. Indeed, the energy of a cluster decreases when evaporated atoms leave it. This can be illustrated using the data shown in Table 1. In this table, the averaged kinetic energy of the evaporated atoms situated in a layer with a lower coordinate x and a thickness of

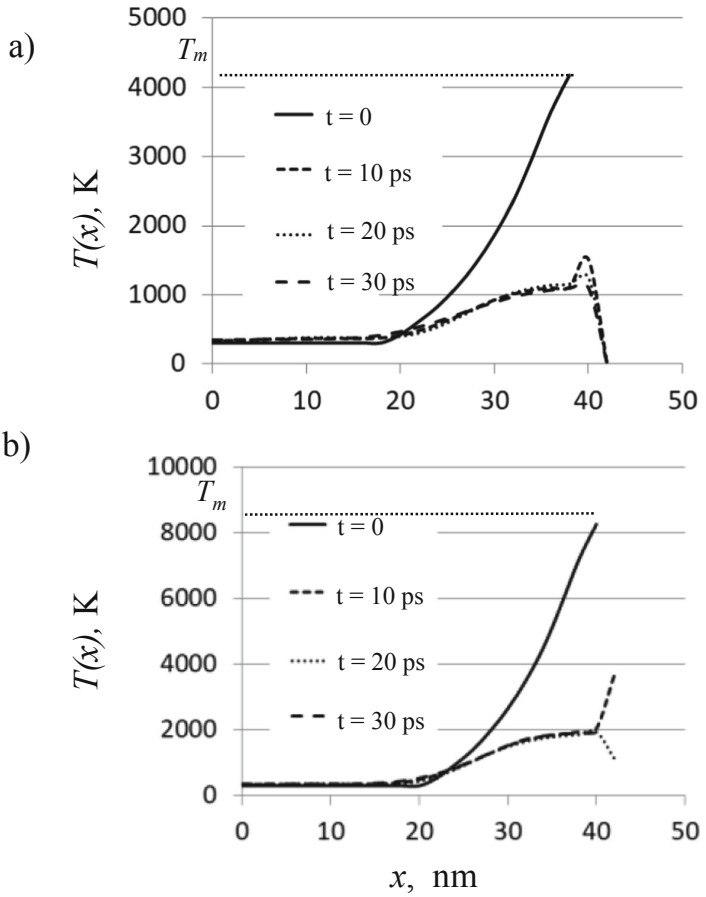

Fig. 3. Temperature distribution $T(x)$ over the cluster thickness for different times t after the absorption of laser radiation. a) T_m = 4200 K, b) T_m = 8400 K. The upper edge of the film corresponds to x = 43–44 nm.

2 nm is calculated and converted to temperature $T(x,t)$. The values of $T(x,t)$ are calculated for the MD frame at the moment t. Then the evaporated atoms are removed from the simulation cluster and the MD simulation continues. This means, for example, that at time t = 12 ps, $T(x,t)$ is calculated only for the atoms that have evaporated during the time period from t = 10 ps to t = 12 ps. Zero values in Table 1 mean that there are no evaporated atoms in the corresponding layer. The coordinate of the upper film edge is approximately 44 nm.

As can be seen from Table 1, the temperature can reach 10^5 K, which corresponds to a kinetic energy of about 10 eV. Since the maximum value of the temperature at the initial moment is less than 1 eV, this means that the evaporated atoms receive energy from collisions with other atoms of the clusters. The release of high-energy atoms from

the film leads to its cooling, which is more significant than in the absence of evaporation. This explains the differences of the temperature distributions shown in Fig. 3a, b.

Evaporated atoms heated to a temperature of about $10^{4\div5}$ K can form regions with plasma, which can significantly affect the absorption of laser radiation. It is worth mentioning here that it was previously assumed that the laser-induced damage of transparent crystals and films can be associated with the formation of a locally plasma region as a result of the matter heating [28–30].

Table 1. The temperature $T(x,t)$ of atoms evaporated from the film, x is the vertical coordinate, t is the time counted from the moment of absorption of laser radiation. Large values of $T(x,t)$ are highlighted in bold.

t, ps →	2	4	6	8	10	12	14	16	18
x,nm	$T(x,t)$, K·104								
46	0	1.8	3.9	3.6	0	0	0	0	0
48	0	3.5	3.1	4.2	1.6	2.7	6.3	5.1	4.3
50	0	2.5	6.9	3.3	0	2.2	0	0	4.5
52	0	2.3	5.9	3.5	0	1.6	4.6	5.8	3.7
54	0	0	8.9	5.9	0	0	3.6	5.4	3.4
56	0	0	7.9	4.9	0	4.2	3.4	4.7	4.5
58	0	0	8.0	5.8	0	0	7.3	6.6	0
60	0	0	7.3	0	0	0	7.1	0	6.4
62	0	0	**10.6**	0	0	0	0	**10.8**	0
64	0	0	0	0	0	0	0	9.8	0
66	0	0	**12.1**	0	0	0	0	0	0
68	0	0	**13.4**	0	0	0	0	0	0

The time dependence of the number of evaporated atoms after the absorption of laser energy is presented in Table 2. The $N(t)$ values are calculated as $N(t) = N_{at}(t + \Delta t) - N_{at}(t)$, where $N_{at}(t + \Delta t)$ and $N_{at}(t)$ are the number of atoms in the cluster at the moments t and Δt respectively, $\Delta t = 2$ ps. Every 2 ps, the evaporated atoms are removed from the simulation area to prevent their possible return to the cluster.

As can be seen from Table 2, evaporation begins within the first few picoseconds after absorption of laser energy and lasts about twenty picoseconds. At $T_m = 4200$ K, the number of the evaporated atoms is negligible for both values of the deposition angle. In the case of $\alpha = 70°$, the evaporation process is more intense than in the case of $\alpha = 0°$. We assume that this is due to differences in the structure of the films.

The dependence of the total number of evaporated atoms on the maximum initial temperature of the clusters is presented in Table 3. The fraction of evaporated atoms does not exceed several percent even for the highest T_m values. This is explained as follows. The cohesion energy of silica is about 20 eV per one SiO_2 group [31], while the maximum additional kinetic energy of an atom at $T_m = 12400$ K is about 1 eV. So only a small part of atoms can receive enough energy to leave the atomistic cluster.

Table 2. The dependence of the number of evaporated atoms *N(t)* on the simulation time *t*, α is the deposition angle, T_m is the maximum initial temperature of the cluster, see Eq. 2.

α	0°		70°	
T_m, K	4200	8400	4200	8400
t, ps	*N(t)*			
0	0	1	0	0
2	1	1	0	1
4	0	1	0	4827
6	2	1630	1	54369
8	1	1280	0	29961
10	0	95	0	9511
12	0	22	1	1361
14	1	30	0	375
16	0	215	0	213
18	1	822	1	41
20	0	128	0	16
22	0	13	0	8
24	0	2	0	0
26	0	0	0	3
28	0	0	0	0
30	0	0	0	6

Table 3. The dependence of the total number of evaporated atoms N_{tot}, on the maximum initial temperature T_m for films deposited at different values of the deposition angle α, *f(%)* is the ratio of N_{tot}, to the initial number of atoms in clusters.

α	0°		70°	
T_m, K	N_{tot},	f(%)	N_{tot},	f(%)
4200	6	0.0	3	0.0
5500	2	0.0	5	0.0
6900	20	0.0	3	0.0
8400	4240	0.17	5	0.0
9600	11570	0.46	100692	4.03
11000	26265	1.05	145543	5.82
12400	48415	1.94	162670	6.51

As expected, the number of evaporated atoms grows with increasing T_m. The dynamic of this growth substantially depends on the deposition angle α. At an angle $\alpha = 70°$, the evaporation process starts more rapidly than at $\alpha = 0°$. This is accompanied by a difference in the evolution of the structure with increasing T_m (Fig. 4). Visual analysis shows that the structure of the film deposited at $\alpha = 0°$ practically does not changes. Whereas in the case of $\alpha = 70°$, an increase in T_m leads to noticeable

changes of the structure. At T_m = 4200 K, the shape of slanted columns changes, and a deep depression is observed in the central part of the cluster. We assume that these differences in the evolution of the structure affect the intensity and rate of the evaporation process in films deposited at $\alpha = 0°$ and $\alpha = 70°$.

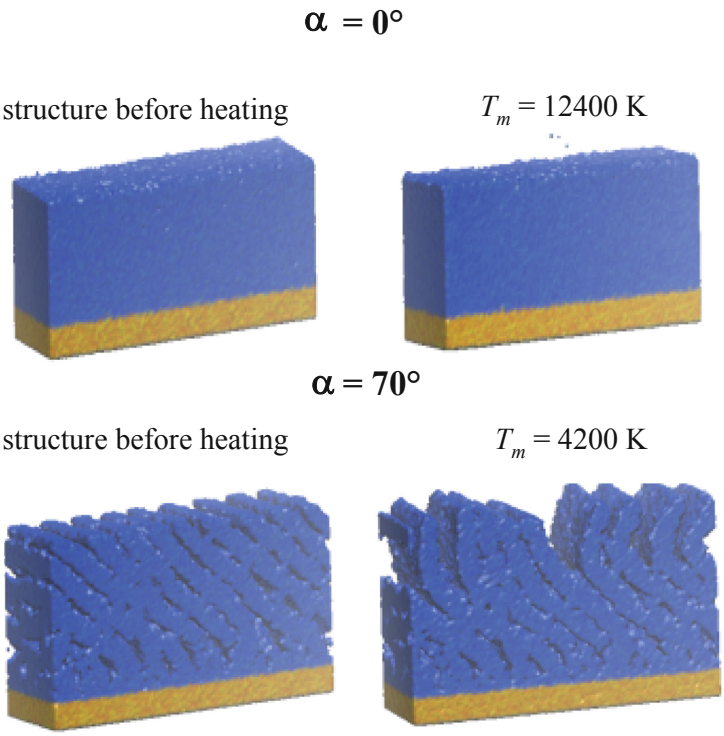

Fig. 4. The structures of the deposited films at different value of the maximum initial temperature T_m.

4 Conclusions

In this work we perform the molecular dynamic simulation of heating and the initial stage of evaporation of silicon dioxide films. The films are deposited at angles $\alpha = 0$ and $\alpha = 70°$ and an energy of incident atoms of 10 eV. Heating is performed by short and intensive laser radiation, which is simulated by the addition of the kinetic energy to atoms at the initial moment. The maximum initial temperature T_m in the top cluster layers vary from $4.2 \cdot 10^3$ K to $1.2 \cdot 10^4$ K.

It was found that the evaporation process begins approximately 2–4 ps after the absorption of laser radiation and lasts approximately 20 ps. The intensive evaporation process begins when T_m exceeds $8 \cdot 10^3$ K. The evaporation process is more intense at $\alpha = 70°$ and is accompanied by a significant change in the film structure.

The work was supported by the Russian Science Foundation (Grant No. 19-11-00053).

References

1. Danson, C., Hillier, D., Hopps, N., Neely, D.: High Power Laser Sci. Eng. **3**, 1–14 (2015)
2. Danson, C.N., et al.: High Power Laser Sci. Eng. **7**(54), (2019)
3. Lawrence Livermore National Laboratory: https://lasers.llnl.gov/
4. Kozlowski, M.R., Chow, R.: Role of defects in laser damage of multilayer coatings. In: SPIE Proceedings Volume 2114, Laser-Induced Damage in Optical Materials: 1993 (1994) https://doi.org/10.1117/12.180876
5. Stolz, C., et al.: Optical Interference Coating, Banff, Canada, (2001)
6. Natoli, J.-Y., Gallais, L., Akhouayri, H., Amra, C.: Appl. Opt. **41**, 3156–3166 (2002)
7. ISO 21254-1, Laser and laser-related equipment - Test methods for laser-induced damage threshold (2011)
8. Jeschke, H.O., Diakhate, M.S., Garcia, M.E.: Appl. Phys. A **96**(1), 33–42 (2009)
9. Wu, C.: Lasers in Materials Science, vol.191/ed. Z.L. Castillejo M., Ossi P. – Springer, 67–100 (2014) https://doi.org/10.1007/978-3-319-02898-9
10. Bai, Q.S.: Molecular simulation and ablation property on the laser-induced metal surface. In: Bai, Q.S. et al. Proc.SPIE. vol. 11063 (2019)
11. Klein, D., Eisfeld, E., Roth, J.: J. Phys. D: Appl. Phys. **54**, 015103 (2021)
12. Yu, J., et al.: Advances in condensed matter physics, 2014, 364627 (2014)
13. Grigoriev, F.V., Zhupanov, V.P., Chesnokov, D.A., Sulimov, V.B., Tikhonravov, A.V.: Lobachevskii Journal of Mathematics **42**(7), 1514–1520 (2021)
14. Keldysh, L.V.: Sov. Phys. JETP **20**, 1307 (1965)
15. Mero, M., Liu, J., Rudolph, W., Ristau, D., Starke, K.: Phys. Rev. B **71**(115109), 1–7 (2005)
16. Jasapara, J., Nampoothiri, A.V.V., Rudolph, W., Ristau, D., Starke, K.: Phys. Rev. B **63** (045117), 1–5 (2001)
17. Grigoriev, F., Sulimov, V., Tikhonravov, A.: J. Non-Cryst. Solids **512**, 98–102 (2019)
18. Grigoriev, F., Sulimov, V., Tikhonravov, A.: Coatings **9**, 568 (2019)
19. Grigoriev, F.V., Sulimov, A.V., Kochikov, I.V., Kondakova, O.A., Sulimov, V.B., Tikhonravov, A.V.: Supercomputer modeling of the ion beam sputtering process: full-atomistic level. In: Proceedings of the Optical Systems Design 2015: Advances in Optical Thin Films V, International Society for Optics and Photonics, Bellingham, WA, USA, 7–10 September 2015, vol. 9627, p. 962708 (2015)
20. Perry, D.L.: Handbook of Inorganic Compounds. CRC Press (2016). https://doi.org/10.1201/b10908
21. Berendsen, H.J.C., Postma, J.P.M., Van Gunsteren, W.F., DiNola, A., Haak, J.R.: J. Chem. Phys. **81**, 3684–3690 (1984)
22. Abraham, M.J., et al.: SoftwareX **1**, 19–25 (2015)
23. Robbie, K., Brett, M.J., Lakhtakia, A.: Nature **384**, 616 (1996)
24. Hawkeye, M.M., Brett, M.J.: J. Vac. Sci. Technol. **25**, 1317 (2007)
25. Voevodin, V.V., et al.: Supercomput. Front. Innov. **6**(2), 4–11 (2019)
26. https://parallel.ru/cluster/lomonosov2.html

27. Leko, V.K., Mazurin, O.V.: Properties of Quartz Glass. Nauka, Leningrad (1985).[in Russian]
28. Carr, C.W., Radousky, H.B., Rubenchik, A.M., Feit, M.D., Demos, S.G.: Phys. Rev. Lett. **92** (8), 087401 (2004)
29. Carr, C. W., Radousky, H. B., Demos, S. G.: Phys. Rev. Lett. **91**, 127402 (2003)
30. Chen, M., Ding, W., Cheng, J., Yang, H., Liu, Q.: Crystal. Appl. Sci. **10**, 6642 (2020)
31. Demuth, T., Jeanvoine, Y., Hafner, J., Angyan, J.G.: J. Phys.: Condens. Mat. **11**, 3833 (1999)